ORIGINAL ARTICLE

Localization of Macrophages in the Human Lung via Design-based Stereology

Patrick S. Hume[1,2], Sophie L. Gibbings[1], Claudia V. Jakubzick[3], Rubin M. Tuder[2], Douglas Curran-Everett[4,5], Peter M. Henson[1,2], Bradford J. Smith[6], and William J. Janssen[1,2]

[1]Division of Pulmonary, Critical Care, and Sleep Medicine, Department of Medicine, and [4]Division of Biostatistics and Bioinformatics, National Jewish Health, Denver, Colorado; [2]Division of Pulmonary Sciences and Critical Care Medicine, [5]Department of Biostatistics and Informatics, Colorado School of Public Health, and [6]Department of Biomedical Engineering, University of Colorado, Anschutz Medical Campus, Aurora, Colorado; and [3]Department of Microbiology and Immunology, Dartmouth College, Hanover, New Hampshire

ORCID IDs: 0000-0002-5861-7375 (P.S.H.); 0000-0002-1583-6762 (B.J.S.); 0000-0002-6397-3454 (W.J.J.).

Abstract

Rationale: Interstitial macrophages (IMs) and airspace macrophages (AMs) play critical roles in lung homeostasis and host defense, and are central to the pathogenesis of a number of lung diseases. However, the absolute numbers of macrophages and the precise anatomic locations they occupy in the healthy human lung have not been quantified.

Objectives: To determine the precise number and anatomic location of human pulmonary macrophages in nondiseased lungs and to quantify how this is altered in chronic cigarette smokers.

Methods: Whole right upper lobes from 12 human donors without pulmonary disease (6 smokers and 6 nonsmokers) were evaluated using design-based stereology. CD206 (cluster of differentiation 206)-positive/CD43$^+$ AMs and CD206$^+$/CD43$^-$ IMs were counted in five distinct anatomical locations using the optical disector probe.

Measurements and Main Results: An average of 2.1×10^9 IMs and 1.4×10^9 AMs were estimated per right upper lobe. Of the AMs, 95% were contained in diffusing airspaces and 5% in airways. Of the IMs, 78% were located within the alveolar septa, 14% around small vessels, and 7% around the airways. The local density of IMs was greater in the alveolar septa than in the connective tissue surrounding the airways or vessels. The total number and density of IMs was 36% to 56% greater in the lungs of cigarette smokers versus nonsmokers.

Conclusions: The precise locations occupied by pulmonary macrophages were defined in nondiseased human lungs from smokers and nonsmokers. IM density was greatest in the alveolar septa. Lungs from chronic smokers had increased IM numbers and overall density, supporting a role for IMs in smoking-related disease.

Keywords: interstitial; alveolar; cigarette smokers; emphysema; morphometry

Resident tissue macrophages are distributed throughout the human lung and play essential roles in maintaining lung homeostasis, host defense, and regulating inflammatory responses (1). Aberrant macrophage function is associated with an array of lung diseases (2, 3), including asthma (4), pulmonary fibrosis (5), pulmonary hypertension (6), and chronic obstructive pulmonary disease (COPD) (7). However, an important knowledge gap in the field exists: no quantitative investigation has been undertaken to clearly define the location and distribution of pulmonary macrophages.

Two main populations of pulmonary macrophages exist: airspace macrophages (AMs) and interstitial macrophages (IMs). AMs are readily retrievable from the airspaces via BAL and, therefore, have been well-studied (8). In comparison, much less is known about IMs because they are located in the tissues. Recent studies using

(Received in original form November 1, 2019; accepted in final form March 20, 2020)

Supported by the NIH grants F32HL145900 (P.S.H.), T32HL007085 (P.S.H.), R35HL140039 (W.J.J.), and R01AI141389 (P.M.H.) and by the MOOR Basic Science travel award from National Jewish Health (P.S.H.).

Author Contributions: Conception and design: P.S.H., C.V.J., P.M.H., B.J.S., and W.J.J. Analysis and interpretation of data: P.S.H., S.L.G., D.C.-E., P.M.H., B.J.S., and W.J.J. Statistical methods and analysis: D.C.-E. Stereological methods: P.S.H. and B.J.S. Acquisition of data: P.S.H. and S.L.G. Pathology review: R.M.T. Drafting and revising manuscript: P.S.H., P.M.H., B.J.S., and W.J.J.

Correspondence and requests for reprints should be addressed to Patrick S. Hume M.D., Ph.D., National Jewish Health, 1400 Jackson Street, Denver, CO 80206. E-mail: humep@njhealth.org.

This article has a related editorial.

This article has an online supplement, which is accessible from this issue's table of contents at www.atsjournals.org.

Am J Respir Crit Care Med Vol 201, Iss 10, pp 1209–1217, May 15, 2020

Originally Published in Press as DOI: 10.1164/rccm.201911-2105OC on March 20, 2020
Internet address: www.atsjournals.org

At a Glance Commentary

Scientific Knowledge on the Subject: Pulmonary airspace and interstitial macrophages play important roles in human health and disease, but their precise anatomic locations remain undefined.

What This Study Adds to the Field: We report the total numbers and locations of macrophages in the healthy human lung and describe how this is altered in chronic cigarette smokers.

whole-lung digests (5, 9–14) have expanded our understanding of pulmonary IMs and suggest that multiple subtypes may exist. However, the roles played by these IM subsets remains largely unknown, as are the precise tissue compartments that they occupy (15). Because tissue microenvironments heavily influence IM function (1, 16), it is suspected that individual macrophage subsets reside in distinct locations and are functionally unique (5, 11). Thus, accurately defining the specific, local microenvironments in which pulmonary macrophages reside is fundamental to understanding macrophage function in health and disease.

Historically, it has been presumed that IMs reside within the alveolar septa (14); however, their presence has also been reported in proximity to the pulmonary vasculature (17) and surrounding the airways (5, 11). Importantly, our knowledge of human pulmonary macrophage location is derived from histologic sections (5, 11, 12, 14, 18). Though instructive, hand-picked images are inherently biased and may not be generalizable to a whole organ (19, 20). This limitation may be addressed using design-based stereology, the gold standard tool for accurate, unbiased estimates of global lung structure (19–22). Accordingly, we apply the principles of design-based stereology to define and quantify the locations of human macrophage subpopulations within specific lung subcompartments.

The primary goal of this study was to determine the location and numbers of pulmonary macrophages in nondiseased human lungs. However, because half of our donor lungs were from chronic smokers, we also sought to determine whether chronic cigarette smoke affects macrophage numbers or alters their locations in tissue. We found that the right upper lobes (RULs) contain over 3 billion macrophages. AMs primarily localized to gas exchange regions, whereas IMs were predominantly located in the alveolar septa. The local density of IMs was greater in the alveolar septa than in the connective tissue surrounding the airways or vessels. Finally, our data show that the total number and density of IMs are increased in the lungs of cigarette smokers versus nonsmokers. Some of the results of these studies have been previously reported in the form of abstracts (23, 24).

Methods

Complete methods, including stereology equations, are provided in the online supplement.

Study Population

Studies used deidentified human lungs procured from organ donors who died from nonpulmonary causes, had clear chest X-rays, and had no history of pulmonary disease. Donors were classified as either nonsmokers or smokers. Smokers had ongoing, daily cigarette smoking for at least 10 pack-years, whereas nonsmokers had never smoked. Hematoxylin and eosin-stained sections from each lung were analyzed by a lung pathologist. Lungs with histologic evidence of acute or chronic disease, including emphysema, were excluded.

Design-based Stereology

The RUL was isolated and inflated with low-melting-point agarose at a constant pressure of 20 cm H_2O, followed by volume displacement (19) to determine RUL volume. Systematic uniform random sampling (25) followed, with ten 1-cm^3 blocks per lung randomly selected, cryoembedded, and cryosectioned. One 40-μm-thick section per block was stained with DAPI and fluorescent antibodies

Table 1. Demographics

Subject	Smoking Status	Sex	Age (*yr*)	Smoking Pack-Years	Pa_{O_2}/FI_{O_2}	RUL Volume (cm^3)
1	NS	F	35	0	370	531
2	NS	F	18	0	427	544
3	NS	F	59	0	263	761
4	NS	M	46	0	308	738
5	NS	M	39	0	357	226
6	NS	M	49	0	242	431
7	S	F	62	40	493	775
8	S	F	66	40	313	329
9	S	F	35	18	291	774
10	S	M	32	13	262	859
11	S	M	44	10	293	252
12	S	M	63	60	379	706
Overall, mean (SD)			46 (15)	15 (21)	333 (75)	577 (223)
NS, mean (SD)			41 (14)	0 (0)	328 (70)	538 (199)
S, mean (SD)			50 (15)	30 (20)	339 (85)	616 (258)
P value (NS vs. S)			0.3	*	0.8	0.6

Definition of abbreviations: NS = nonsmoker; RUL = right upper lobe; S = smoker.
**P* value is not reported for smoking pack-years because the populations were selected to be different.

against human CD206 (cluster of differentiation 206), CD43, and elastin (*see* Table E1 in the online supplement for antibody information). Four-channel fluorescent images were captured using an Olympus BX53 microscope controlled by Visiopharm newCAST stereology software. Slides were randomized and blinded throughout morphometry analysis.

Area point counting (26) was performed to calculate the volume fraction of the following subtissue spaces: diffusing airspaces, alveolar septa, vessel walls, vessel lumens, airway walls, and airway lumens. The "alveolar septa" included septa from alveoli, alveolar ducts, and respiratory bronchioles. Airway/vessel walls included the surrounding adventitia. Only small airways/vessels (defined as <2 mm in diameter) were of sufficient abundance for sampling. Individual subcompartment volumes were calculated by multiplying their respective volume fraction by total RUL volume.

Elastin and DAPI staining were visualized in a low-magnification image and the section was manually partitioned into subregions of diffusing lung tissue, vessels, or airways. Approximately 15 randomly positioned, high-power, 25-μm-thick three-dimensional (3D) *z*-stacks were captured per region of interest, per slide. Manual cell counting using the principle of the optical disector (27, 28) determined the density of AMs and IMs per subtissue volume. Multiplying subtissue macrophage density by total subtissue volume yielded the total number of IMs or AMs per tissue compartment, per RUL. The overall IM or AM density is a volume-weighted average of the individual subtissue densities.

Flow Cytometry

After volume displacement to determine the precise tissue volume, fresh human lung tissue from four healthy subjects was enzymatically digested and then stained for flow cytometry, as described in detail in the online supplement.

Statistical Analysis

We used a general linear model to assess the impact of sex, age, smoking status, and location on IM total number and density (PROC MIXED; SAS/STAT software package, version 9.4; SAS Institute). This mixed-effects model used an unstructured variance matrix and accounted for measurements from three locations per lung (alveolar septa, airway wall, and vessel wall). Preliminary analyses demonstrated that: *1*) a $\log_{10}$ transformation of IM total number and density stabilized the variance; *2*) sex ($P \geq 0.74$) and age ($P \geq 0.10$) did not impact IM total number or density, these terms were dropped from the final statistical model; and *3*) smoking did not alter the effect of location on IM total number or density ($P \geq 0.18$). The variables included in the final general linear model were smoking status (yes or no) and anatomic location (alveolar septa, airway wall, and vessel wall). Prism 8 (GraphPad) was used to perform a two-tailed *t* test for single-variable comparisons. Unless otherwise stated, all data are presented as mean (SD) and *P* values refer to the general linear model. Because the goal was to newly define the distribution of macrophages, we did not control for multiple comparisons.

Results

Human Lung Tissue

Morphometric analysis was performed on 12 human donor lungs; full demographics are shown in Table 1. Lungs were distributed evenly by sex and smoking

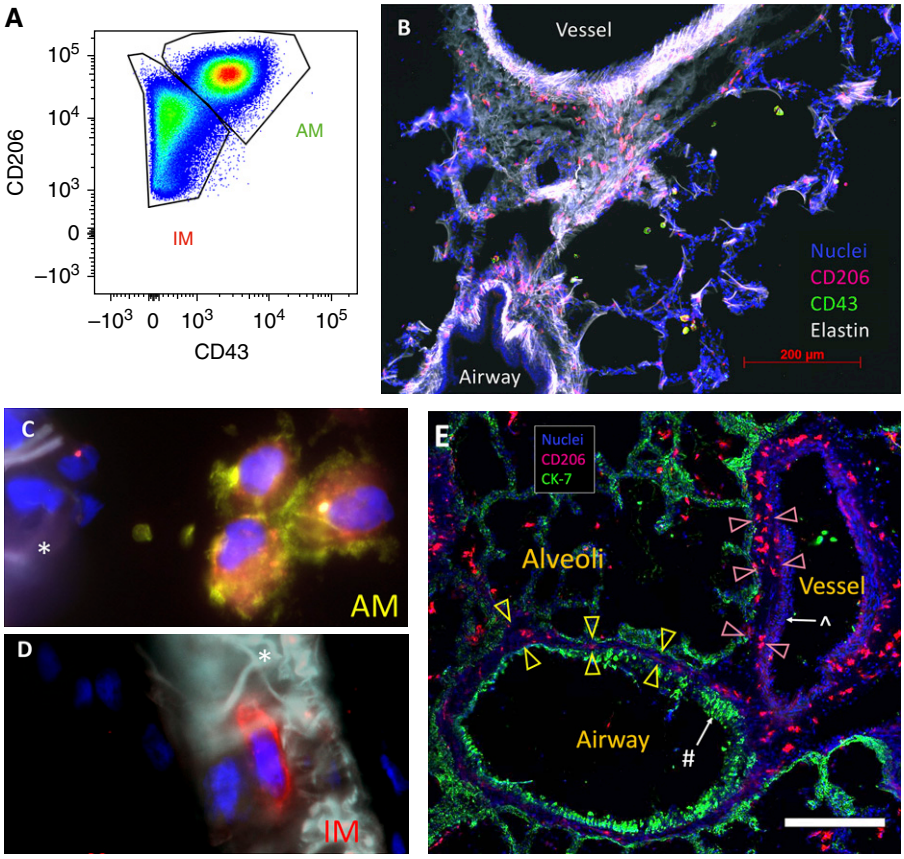

Figure 1. Identification of pulmonary macrophage populations. (*A*) Flow cytometry of CD45 (cluster of differentiation 45)-positive/CD3$^-$/CD19$^-$/CD15$^-$/DAPI$^-$ myeloid cells from human lung digest illustrating that airspace macrophages (AMs) and interstitial macrophages (IMs) are CD206$^+$ but only AMs are CD43$^+$. (*B–E*) Immunofluorescent staining of human lung tissue to localize AMs and IMs. (*B*) The luminal airway epithelial surface was elastin negative, whereas the vessel wall was elastin positive with a characteristic appearance, enabling the rapid, visual distinction between airways and vessels. CD206$^+$/CD43$^+$ AMs (red and green, respectively) are in the airspaces and CD206$^+$/CD43$^-$ IMs (red) are easily identified in the interstitium. (*C* and *D*) High-power magnification shows CD206$^+$/CD43$^+$ AMs (red and green, respectively) located in the alveolus (*C*) and CD206$^+$/CD43$^-$ (red) IMs located within the septum (*D*). The asterisks denote the alveolar septum. (*E*) Demonstration of airways and vessel wall compartments. CK-7 (green) highlights epithelium. CD206 (red) identifies macrophages. Nuclei are shown in blue. The # symbol denotes airway epithelium, whereas the ^ symbol denotes vessel endothelium. Airway-associated IMs are located within the subepithelial tissue (between yellow arrowheads), whereas vessel-associated IMs are within the subendothelial tissue (between pink arrowheads). Scale bar, 400 μm. CK = cytokeratin.

status. Smokers had a mean cigarette smoke exposure of 30 (SD, 20) pack-years that did not vary significantly by sex. The average subject age was 46 (SD, 15) years; age did not vary significantly by sex or smoking status. Likewise, the average (330 [SD, 80]) Pa_{O_2}/FI_{O_2} ratio and RUL (580 [SD, 220]) cm^3) volume were similar across sex and smoking status.

Identification of Pulmonary Macrophages

Before embarking on design-based stereology, we performed flow cytometry on digested human lung tissue to identify highly specific surface markers to detect macrophages and distinguish IMs from AMs. In line with recent publications (14, 29, 30), we confirmed that CD206, the mannose receptor, was highly expressed on all lung macrophages. We also confirmed that CD43 (also known as leukosialin) was expressed on AMs (31) but not IMs (Figures 1A and *see* Figure E1A). Immunofluorescent staining for CD206 and CD43 on cryosections readily distinguished IMs from AMs (*see* Figures 1B–1D).

Design-based Stereology

Care was taken to design a stereology approach capable of quantifying cellular subtypes within specifically defined lung subcompartments. Lung tissue was isolated and randomly sampled via the workflow summarized in Figures E2A–E2E. After immunostaining, whole-slide imaging was used to visually define regions of interest for airways, vessels, or diffusing subtissues, as shown in Figures E2F and E2G. This subsampling approach was an innovation for this project that enabled detailed macrophage quantitation per specific lung subtissue. Next, software-guided image acquisition of each region of interest was performed and IMs were readily observed in the walls of septa (*see* Figure 1D), airways (Figure 2A), and vessels (*see* Figure 2B). Macrophage subpopulations were manually counted within 3,485 *z*-stack images using the optical disector to estimate macrophage locations. Shrinkage

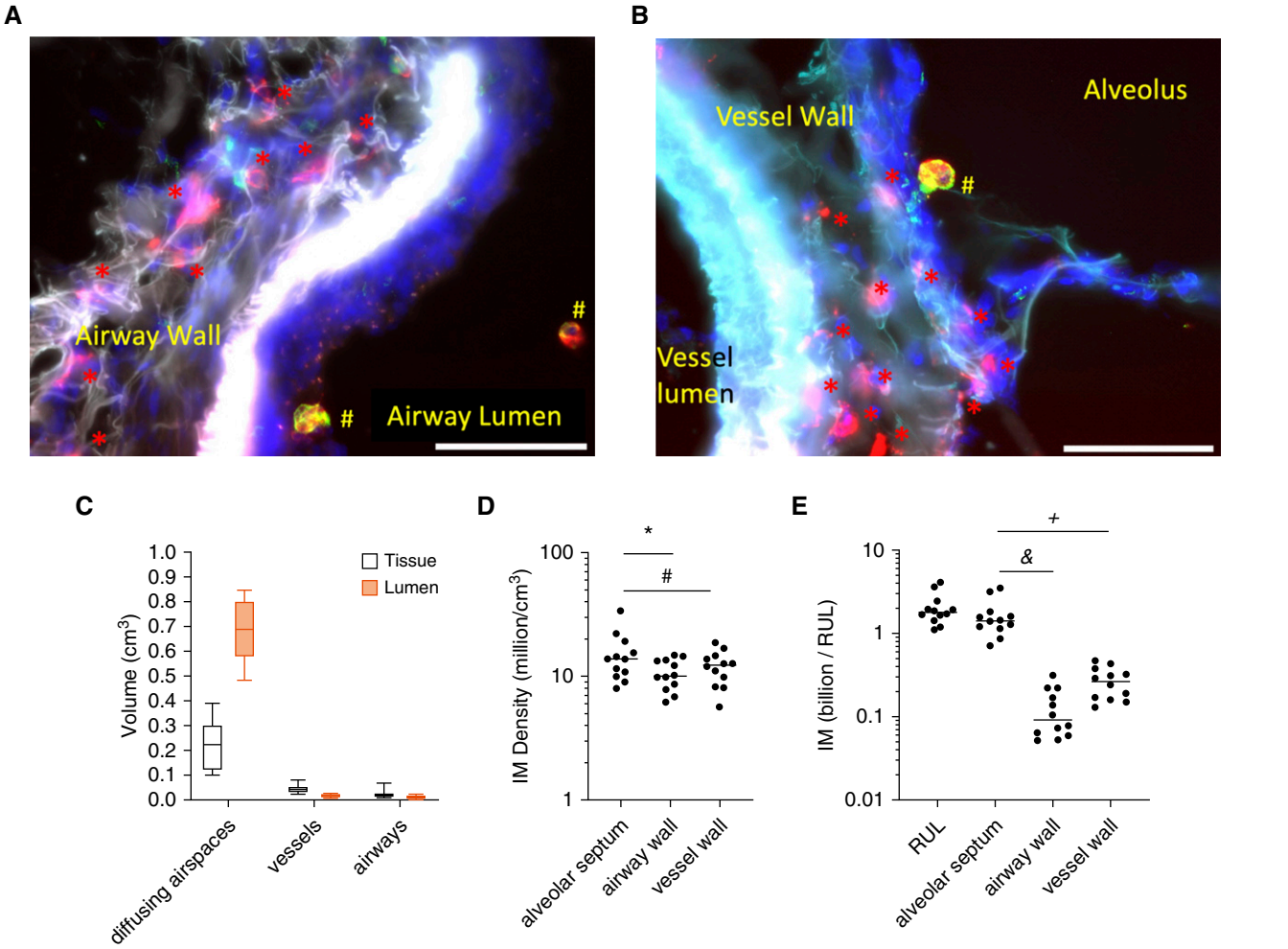

Figure 2. Quantification of interstitial macrophages (IMs) in lung subcompartments using stereology. (*A*) CD206 (cluster of differentiation 206)-positive IMs (red asterisks) are identified within the airway wall with $CD206^+/CD43^+$ airspace macrophages (red and green make yellow; #) located in the airway lumen. (*B*) Red $CD206^+$ IMs visualized within the vessel wall and $CD206^+/CD43^+$ airspace macrophages (red and green make yellow; #) are visualized within the alveolus. Scale bars, 50 μm. (*C*) Volume fraction of each lung subcompartment was calculated via stereology. Diffusing airspaces consisted of alveoli, alveolar ducts, and respiratory bronchioles. (*D*) Density of IMs in lung subcompartments. $^*P = 0.02$ and $^\#P = 0.06$. (*E*) Total number of IMs counted in human lung per subcompartment. $^\&P < 0.0001$ and $^+P < 0.003$. RUL = right upper lobe.

in the *z*-dimension was anticipated (32, 33) and quantified for every slide, with an average shrinkage to be 0.6 (SD, 0.1) of the original section height.

Localization of IMs in Human Lung

Vessel and airway walls were defined as the space spanning the luminal endothelium (vessel) or epithelium (airway) through the surrounding connective tissues. The alveolar septum was defined as the tissue dividing alveoli or other diffusing airspaces (including respiratory bronchioles and alveolar ducts). IMs were identified in three discrete regions: the alveolar septa (*see* Figure 1D), the subepithelial airways, and the subendothelial vessels (*see* Figure 1E). Elastin staining was included in all morphometry sections to visually distinguish airways from vessels (*see* Figure 1B). A pulmonary pathologist analyzed representative immunofluorescent samples to confirm that airways, vessels, and diffusing tissues were readily distinguishable and clearly identified.

As detailed in Table 2, within the RUL, the alveolar septa occupied 110 (SD, 57) cm^3, the vessel walls comprised 23 (SD, 9) cm^3, and the airway walls comprised 13 (SD, 9) cm^3. The volumes occupied by the lumens of gas exchange regions, the conducting airways, and the vessels were 410 (SD, 210) cm^3, 7 (SD, 6) cm^3, and 9 (SD, 6) cm^3, respectively. The volume fraction of each lung compartment (*see* Figure 2C) is consistent with prior observations (34).

The optical disector was used to quantify macrophage populations by location. The density of IMs was determined for each anatomic compartment for each lung (*see* Figure 2D). The average density of IMs within the alveolar septa was 22% greater than within the vessel walls (95% confidence interval [CI], 1% less to 51% greater; $P = 0.06$) and 36% greater than the airway walls (95% CI, 5–76% greater; $P = 0.02$). Leveraging the power of unbiased stereology, the total number of each macrophage per subpopulations per RUL were calculated. On average, a total of 2.1 (SD, 0.9) billion IMs exist in the RUL (*see* Figure 2E). Over 75% of the IMs were located in the alveolar septa (1.6 [SD, 0.9] billion). There were 0.27 (SD, 0.11) billion IMs in the vessel wall and 0.13 (SD, 0.09) billion in the airway walls. The large numbers of IMs in the alveolar septa reflected the fact that the septa accounted for 22% of total lung volume, compared with 4% or 2% of total lung volume occupied by the vessel or airway walls, respectively. Finally, we compared the overall IM density estimated by stereology to that of flow cytometry of digested lung (quantified via normalization to bead counts) taken from both proximal and distal lung locations (*see* Figure E5). Whereas stereology estimated 4.0 (SD, 1.8) $\times 10^6$ IMs/cm^3, flow cytometry estimated dramatically fewer, 0.1 (SD, 0.1) $\times 10^6$ IMs/cm^3.

Chronic Cigarette Smoking Increases Pulmonary IM Number

We next compared the lungs of nonsmokers to smokers. As shown Figure 3A, the RUL volumes were equivalent. Similarly, there was no difference between the volume of alveolar septa, airway walls, or vessel walls (*see* Figure 3B). There were 56% more (95% CI, 5–132%; $P = 0.03$) IMs in the lungs of chronic cigarette smokers than nonsmokers (2.6 [SD, 1.0] vs. 1.5 [SD, 0.4] billion, respectively) (*see* Figure 3C). This was due to an elevated volume density of IMs in smokers by 36% (95% CI, −1% to 88%; $P = 0.06$) (*see* Figure 3D). In smokers, there was no correlation between IM numbers or IM density and either sex or number of pack-years.

Localizing AMs in Human Lung

The distribution of AMs between the conducting airway lumens and the gas-exchanging airspaces has not been previously described. Thus, although our morphometry protocol was primarily tailored to localize IMs, we also documented the location of AMs. Using the optical disector, we estimated the RUL contains 1.4 (SD, 0.9) billion AMs (Figure 4A), which is not significantly different from the total number of IMs, 2.1 (SD, 0.9) billion IMs ($P = 0.1$). Over 97% of AMs were present in the diffusing airspaces (1.4 [SD, 0.9] $\times 10^9$ AMs) versus the airway lumens (9.1 [SD, 9.4] $\times 10^6$ AMs). This effect was driven by the vastly larger volume occupied by gas exchange regions than by the conducting airways (410 [SD, 210] cm^3 vs. 7 [SD, 6] cm^3, respectively). The local density of AMs in diffusing lumens (4.7 [SD, 4.0] million AMs/cm^3) was significantly greater than in the airway lumens (1.6 [SD, 1.5] AMs/cm^3), as shown in Figure 4B ($P = 0.02$, by *t* test). Of note, inflation of the RUL with agarose

Table 2. Stereology Results

	Volume Fraction	Total Volume (cm^3)	IM Density (*Millions*/cm^3)	Total IMs (*Billions*)	AM Density (*Millions*/cm^3)	Total AMs (*Billions*)
Diffusing airspaces	0.90 (0.03)	530 (210)	—	—	—	—
Septa	0.22 (0.11)	110 (57)	15 (7)	1.6 (0.9)	—	—
Lumen	0.68 (0.12)	410 (210)	—	—	4.7 (4.0)	1.4 (0.9)
Vessels	0.06 (0.02)	32 (13)	—	—	—	—
Wall	0.04 (0.02)	23 (9)	12 (4)	0.3 (0.1)	—	—
Lumen	0.02 (0.02)	9 (5)	—	—	—	—
Airways	0.035 (0.02)	20 (12)	—	—	—	—
Wall	0.024 (0.02)	13 (9)	11 (3)	0.1 (0.1)	—	—
Lumen	0.012 (0.01)	7 (6)	—	—	1.6 (1.5)	0.01 (0.01)
Total	1.0	580 (220)	4.0 (1.8)	2.1 (0.9)	2.8 (2)	1.4 (0.9)

Definition of abbreviations: AM = airspace macrophage; IM = interstitial macrophage.
All values are presented as mean (SD).

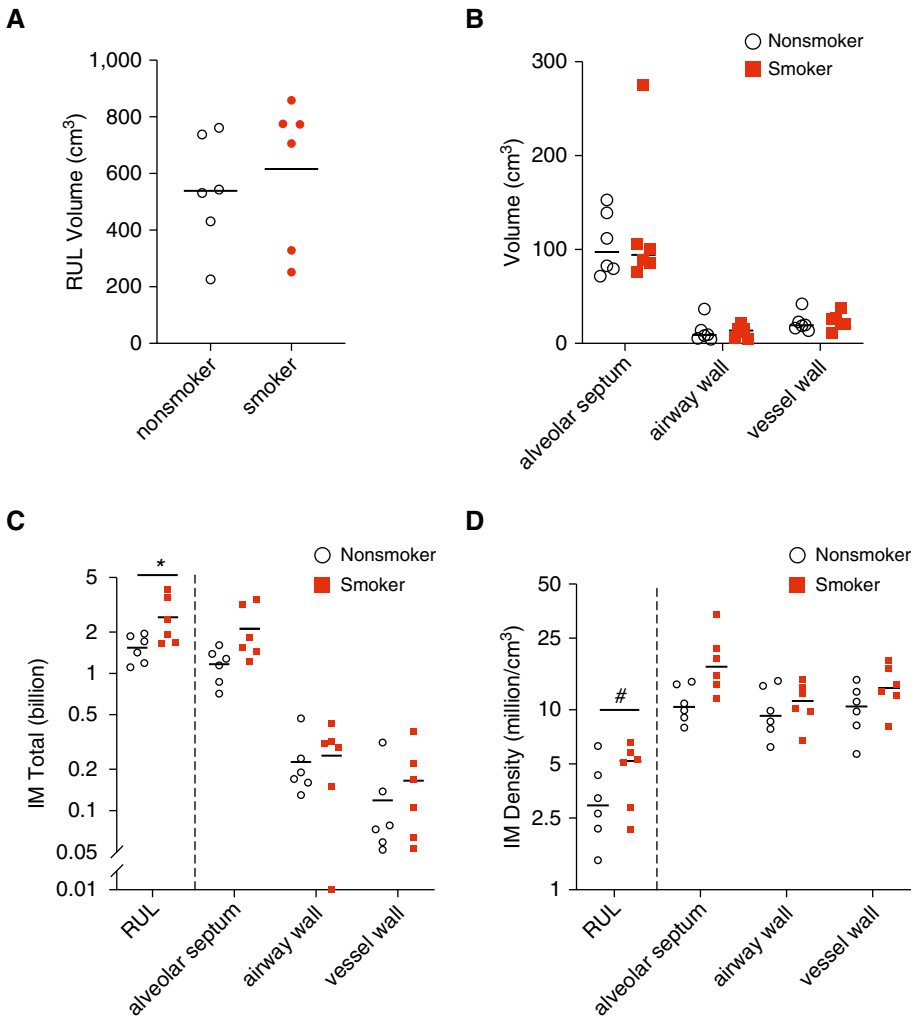

Figure 3. Comparison of interstitial macrophage (IM) number and location in nonsmokers versus chronic cigarette smokers. (*A* and *B*) Lungs were structurally similar between smokers and nonsmokers with equivalent total volume (*A*) and volume of lung subcompartments (*B*). Plotted is mean ± SEM. (*C*) IM total number was increased overall in cigarette smokers. (*D*) IM density was increased overall in cigarette smokers with a trend toward increase in the alveolar septa. (*C* and *D*) $^{*}P = 0.03$ and $^{\#}P = 0.06$. The *y*-axis is plotted as $\log_{10}$ scale. RUL = right upper lobe.

was necessary for accurate lung architecture identification. It is possible that this may have pushed some AMs from the airway lumens distally to the alveoli. Surprisingly, there was no difference in the total number or local density of AMs between smokers and nonsmokers (*see* Figures 4C and 4D).

Sex and Age Did Not Significantly Impact Macrophage Distribution

Differences in immune function have been reported between males and females, including differential macrophage phagocytic activity and cytokine production (35). Thus, we included tissue from an equal number of males and females. We found no difference in total RUL volumes between the men and women in our sample set (*see* Figure E3A). Likewise, the total number, density, and distribution of IMs and AMs did not vary by sex (*see* Figures E3B and E3C). Finally, there was no relationship between age and IM or AM numbers or distribution (*see* Figures E4A–E4C).

Discussion

Recent studies have highlighted the complexity of pulmonary IMs, which potentially play yet undiscovered roles in many human diseases, including the development of emphysema. However, due to the inherently destructive nature of harvesting IMs via whole-lung digestion, all information regarding location is lost. Based on a growing body of evidence that suggests that microenvironment dictates macrophage function (1, 5, 16), our primary goal was to define the specific locations of pulmonary macrophages in human lung tissue using rigorous, unbiased methodology. Herein, we used design-based stereology to manually count the number of fluorescently labeled AMs or IMs within predefined pulmonary subtissue regions. Our findings demonstrate heterogeneous distribution of macrophages throughout the lungs. The alveolar septa contain the greatest number of IMs (approximately 76%) and also have the highest density of these cells. We also highlight an overall increase in IM numbers in chronic cigarette smokers.

Design-based stereology is the gold standard approach for microscopy-based lung morphometry because it allows for assumption-free quantitation of 3D tissues (21). Unlike flow cytometry, no cells are lost in the process of digestion and cellular location is preserved. Likewise, semiquantitative microscopy approaches, such as counting the number of cells per high-power field-of-view, do not consider the size or orientation of a cell. Such factors potentially bias a cell to being more or less likely to appear within any one 2D frame (20). Furthermore, without careful stereological characterization of tissue volumes, cell population estimates may be skewed by unanticipated volumetric changes (e.g., due to anatomical differences). Thus, to eliminate potential biases, we used the optical disector stereological probe with careful characterization of anisotropic tissue shrinkage to meticulously count the number of cells within 3D tissue thicknesses.

As determined by stereology, IMs were most abundant in the alveolar septa (78% of all IMs), in accordance with the abundance of septal tissue in human lung (76% of total lung tissue volume). An unanticipated finding is that the density of IMs located within the alveolar septum was also greater than within the vessel or airway walls. The factors that determine local macrophage density remain unknown but are likely closely related to macrophage function. Our findings provide motivation for future studies that investigate how and why local IM density varies between tissue compartments, particularly because

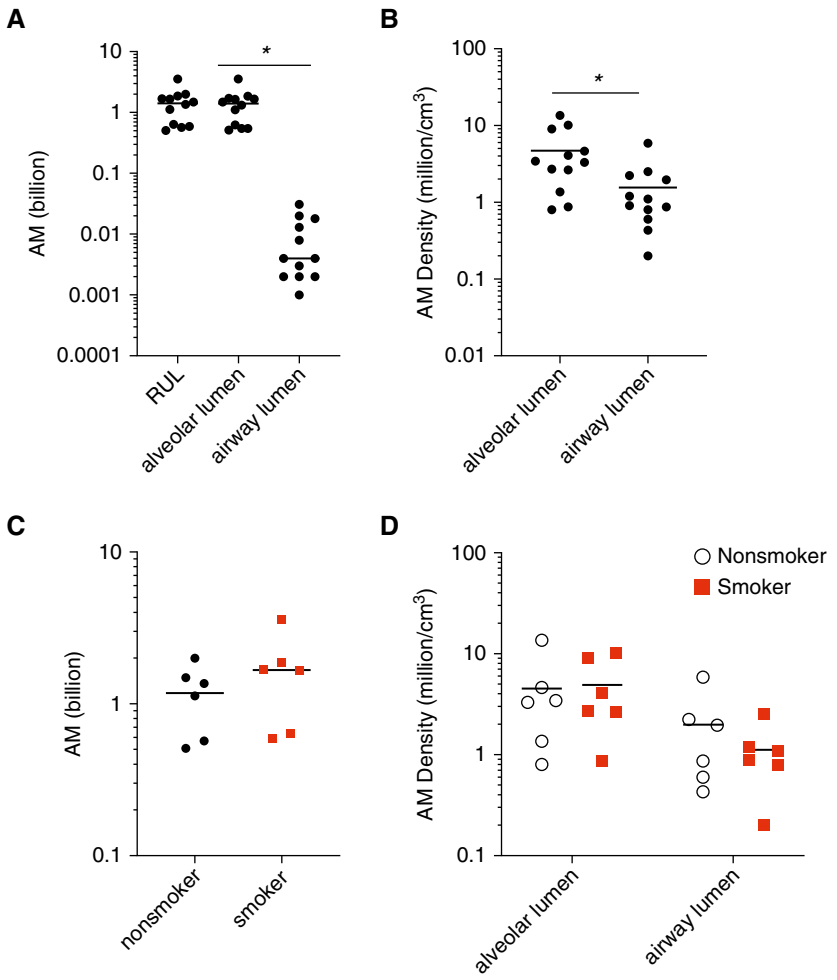

Figure 4. Quantification of airspace macrophages (AMs) in human lung. (*A*) The overwhelming majority of AMs were present in the diffusing airspaces rather than the airway lumens. (*B*) The density of AMs in the diffusing airspaces was significantly greater than that within the airway lumens (by *t* test). (*C*) Total AM number was equivalent in nonsmokers and smokers. (*D*) AM density in tissue subcompartments was not different in smokers versus nonsmokers. Diffusing airspace was defined to include alveoli, alveolar ducts, and respiratory bronchioles. $^*P < 0.05$. The *y*-axis is plotted as $\log_{10}$ scale. RUL = right upper lobe.

microenvironment affects macrophage function (1).

By extrapolating our data from the RUL, we estimate that the healthy human lung contains 14×10^9 AMs. This number compares favorably to a prior morphometry study that estimated 23×10^9 AMs (36). We may have estimated fewer cells because of the implementation of fluorescent antibodies to identify AMs. In comparison, our estimation of AM density is roughly 10-fold greater than previously suggested by another study (37), with the caveat being that prior investigation did not use a 3D sampling probe.

It is accepted that the total numbers of AMs are increased in BAL fluid from human smokers (38, 39) and COPD patients (40). A prior study (41) reported an approximately 1.7-fold increase in the number of AMs in smokers versus nonsmokers by histology. Notably, that study did not use a 3D sampling probe and likely included tissue from patients with mild COPD. So, we sought to estimate AM number using the current state-of-the-art stereology technique in tissue obtained from human smokers without evidence of COPD. Surprisingly, our study showed that AM numbers were similar between nonsmokers and smokers. One possibility that could reconcile previously observed increases in AM numbers by lavage, but not by our quantitative tissue histology, is that cigarette smoke may make AMs less adherent (39) and, therefore, render them more retrievable by lavage. An alternative possibility is that brief withdrawal from cigarette smoke normalized AM numbers. In this context, we note that all donors were on mechanical ventilation for a brief period of time (all <72 h) before organ procurement. Future studies will be necessary to investigate this discrepancy.

Because others have reported impaired macrophage function (42) and increased numbers near the small airways in COPD patients (43), we sought to understand how IM numbers and densities vary in different tissue subcompartments between smokers and nonsmokers without COPD. We observed no differences in IM numbers near the small airways. Interestingly, pairwise comparisons via *t* distribution demonstrated that IM density was greater in the alveolar septa of smokers versus nonsmokers (19.3 [SD, 8.0] vs. 11.0 [SD, 2.6] million/cm^3, respectively; $P = 0.036$). However, multiple subtissue compartments were measured per sample, and so we created a mixed-effect model to account for these repeated measurements. Ultimately, this model did not identify a key relationship between smoking status and IM number or density within any one location, including the alveolar septa. We suspect that variability between subjects (i.e., some subjects had more IMs in every tissue subcompartment) may have limited our ability to detect a difference within any one subcompartment. Ultimately, our mixed-effect model did confirm an overall increase in total IM number and overall density in cigarette smokers versus nonsmokers across all tissue subcompartments.

Studies have shown that CD206$^+$ staining identifies all lung macrophages (14, 29, 30) and distinguishes them from CD206$^-$ intravascular monocytes (29). Migrating lung tissue monocytes may gain weak CD206 expression (29) but at a sufficiently low level such that lung tissue monocytes are also generally considered CD206$^-$ (14, 44). Similarly, CD43 has been shown to distinguish AMs from IMs (31). To verify our markers, we performed multiparameter flow cytometry using standardize protocols (14, 30) and confirmed that AMs (CD206$^+$/CD43$^+$) and IMs (CD206$^+$/CD43$^-$) could be easily distinguished (*see* Figure E1B). Of note, some CD206$^-$ lymphocytes can express

CD43 (45), so $CD206^-/CD43^+$ cells were not classified as macrophages. Finally, a small population of $CD206^+/CD1c^+$ dendritic cells has been reported to exist in the lungs (31). Flow cytometry demonstrated that $CD1c^+$ cells accounted for <5% of the total $CD206^+/CD43^-$ population and <1% of the $CD206^+/CD43^+$ population (*see* Figure E1C). Furthermore, when we stained lung sections for CD1c and CD206, dual-positive cells were extremely rare (*see* Figure E1D). The abundance of this dendritic cell population (<5%) was less than the SEM calculated for the total number of IMs observed (12%), so it is unlikely to have significantly skewed our results. Of the macrophages observed in the alveolar septum, 1.7% (SD, 0.4%) were $CD43^+$. Likewise, 1.6% (SD, 0.2%) of macrophages in the alveolar lumen were $CD43^-$. The low frequency of these cells precluded robust stereologic assessment and they were excluded from data analysis. Finally, there has been recent interest in distinguishing free AMs from sessile AMs attached to the alveolar wall (46). Though we observed both AM morphologies, we ultimately did not record AM subtypes out of concern that agarose inflation may have disturbed local AM attachment.

In addition to estimating the density of IMs with stereology, we also quantified them in lung digests using flow cytometry (*see* Figure E5A). Notably, the density of IMs was approximately 40-fold less when estimated by flow cytometry of digested lung tissue. This highlights a potential caveat to using flow cytometry as a sole means of quantifying cell numbers from lung digests. Notably, a prior study highlighted 10-fold fewer alveolar epithelial type 2 cells when quantified by flow cytometry versus stereology (47). This discrepancy may be due to incomplete liberation of IMs during digestion or to cell death during processing. Accordingly, our work highlights the value of unbiased stereology for quantification of cell number and location within 3D tissues.

Our study included 12 lungs. Although this sample size may seem small, the difficulty of obtaining nondiseased human lungs and the labor-intensive nature of stereology precluded analysis of additional specimens (cells were manually counted in over 290 four-channel fluorescent *z*-stack images per RUL). In fact, the overall sample size of our cohort exceeds those of other human pulmonary stereological studies (34, 48, 49). It was necessary to focus exclusively on the RUL for each lung given our need to share precious human lung tissue with other research groups. Furthermore, in many cases, left lungs were successfully transplanted and unavailable for study.

Because our approach leveraged the principle of uniform random sampling, some subcompartments of the lung were not evaluated. For example, structures occupying a relatively small volume of the total lung, including large airways/vessels, intralobular septa, or the pleura, were not represented. Conversely, alveolar tissue and small vessels/airways (defined at <2 mm diameter) represent a majority of lung tissue. Though we and others (18) have visualized IMs around large vessels/airways and near the pleural surface, such tissue spaces constitute less than 1% of the total lung volume (34) and were excluded from analysis.

Conclusions

Our study defined the subtissue locations of pulmonary macrophages in the human lung using unbiased stereology, the state-of-the-art method for lung structure analysis. We report that the local tissue density of IMs is greatest in the alveolar septa but that IMs are also readily found in proximity to the small airways and vessels. Furthermore, chronic cigarette smoke exposure results in an increase in overall IM numbers and density with a trend toward enrichment within the alveolar septa. Our future studies will be directed toward understanding the roles macrophage subtypes play in specific subtissue locations. Specifically, given our observed enrichment of IMs in the lungs of chronic smokers, we propose IMs (specifically the IMs located within the alveolar septa) play a key, undefined role in the development of emphysema. Our results highlight that IMs are distributed widely throughout the lung. Given the likelihood that individual IM subpopulations localize to specific tissue subcompartments (5), our work serves as a foundation for future experiments designed to elucidate the function of macrophage subpopulations and the mechanisms by which their locations contribute to pathology. ■

Author disclosures are available with the text of this article at www.atsjournals.org.

Acknowledgment: The authors thank Stacey Thomas; Jazalle McClendon; Alexandra McCubbrey, Ph.D.; Kara Mould, M.D.; Carlyne Cool, M.D.; and Kayo Okamura for their assistance. This project was developed with the assistance of the 2017 Stereology Workshop in Bern, Switzerland, and the authors thank all attendees for their input.

References

1. Amit I, Winter DR, Jung S. The role of the local environment and epigenetics in shaping macrophage identity and their effect on tissue homeostasis. *Nat Immunol* 2016;17:18–25.
2. Murray PJ, Wynn TA. Protective and pathogenic functions of macrophage subsets. *Nat Rev Immunol* 2011;11:723–737.
3. Wynn TA, Vannella KM. Macrophages in tissue repair, regeneration, and fibrosis. *Immunity* 2016;44:450–462.
4. Sabatel C, Radermecker C, Fievez L, Paulissen G, Chakarov S, Fernandes C, *et al*. Exposure to bacterial CpG DNA protects from airway allergic inflammation by expanding regulatory lung interstitial macrophages. *Immunity* 2017;46:457–473.
5. Chakarov S, Lim HY, Tan L, Lim SY, See P, Lum J, *et al*. Two distinct interstitial macrophage populations coexist across tissues in specific subtissular niches. *Science* 2019;363:eaau0964.
6. Pullamsetti SS, Savai R. Macrophage regulation during vascular remodeling: implications for pulmonary hypertension therapy. *Am J Respir Cell Mol Biol* 2017;56:556–558.
7. Wang Y, Xu J, Meng Y, Adcock IM, Yao X. Role of inflammatory cells in airway remodeling in COPD. *Int J Chron Obstruct Pulmon Dis* 2018; 13:3341–3348.
8. Lehnert BE, Valdez YE, Holland LM. Pulmonary macrophages: alveolar and interstitial populations. *Exp Lung Res* 1985;9:177–190.
9. Bedoret D, Wallemacq H, Marichal T, Desmet C, Quesada Calvo F, Henry E, *et al*. Lung interstitial macrophages alter dendritic cell functions to prevent airway allergy in mice. *J Clin Invest* 2009;119: 3723–3738.
10. Atif SM, Gibbings SL, Jakubzick CV. Isolation and identification of interstitial macrophages from the lungs using different digestion enzymes and staining strategies. *Methods Mol Biol* 2018;1784:69–76.
11. Gibbings SL, Thomas SM, Atif SM, McCubbrey AL, Desch AN, Danhorn T, *et al*. Three unique interstitial macrophages in the murine lung at steady state. *Am J Respir Cell Mol Biol* 2017;57:66–76.
12. McCubbrey AL, Barthel L, Mohning MP, Redente EF, Mould KJ, Thomas SM, *et al*. Deletion of c-FLIP from $CD11b^{hi}$ macrophages prevents development of bleomycin-induced lung fibrosis. *Am J Respir Cell Mol Biol* 2018;58:66–78.

13. Dewhurst JA, Lea S, Hardaker E, Dungwa JV, Ravi AK, Singh D. Characterisation of lung macrophage subpopulations in COPD patients and controls. *Sci Rep* 2017;7:7143.
14. Yu Y-RA, Hotten DF, Malakhau Y, Volker E, Ghio AJ, Noble PW, *et al*. Flow cytometric analysis of myeloid cells in human blood, bronchoalveolar lavage, and lung tissues. *Am J Respir Cell Mol Biol* 2016;54:13–24.
15. Liegeois M, Legrand C, Desmet CJ, Marichal T, Bureau F. The interstitial macrophage: a long-neglected piece in the puzzle of lung immunity. *Cell Immunol* 2018;330:91–96.
16. Gosselin D, Link VM, Romanoski CE, Fonseca GJ, Eichenfield DZ, Spann NJ, *et al*. Environment drives selection and function of enhancers controlling tissue-specific macrophage identities. *Cell* 2014;159:1327–1340.
17. Pugliese SC, Kumar S, Janssen WJ, Graham BB, Frid MG, Riddle SR, *et al*. A time- and compartment-specific activation of lung macrophages in hypoxic pulmonary hypertension. *J Immunol* 2017; 198:4802–4812.
18. Eapen MS, Hansbro PM, McAlinden K, Kim RY, Ward C, Hackett TL, *et al*. Abnormal M1/M2 macrophage phenotype profiles in the small airway wall and lumen in smokers and chronic obstructive pulmonary disease (COPD). *Sci Rep* 2017;7:13392.
19. Ochs M, Mühlfeld C. Quantitative microscopy of the lung: a problem-based approach. Part 1: basic principles of lung stereology. *Am J Physiol Lung Cell Mol Physiol* 2013;305:L15–L22.
20. Weibel ER, Hsia CCW, Ochs M. How much is there really? Why stereology is essential in lung morphometry. *J Appl Physiol (1985)* 2007;102:459–467.
21. Hsia CCW, Hyde DM, Ochs M, Weibel ER; ATS/ERS Joint Task Force on Quantitative Assessment of Lung Structure. An official research policy statement of the American Thoracic Society/European Respiratory Society: standards for quantitative assessment of lung structure. *Am J Respir Crit Care Med* 2010;181:394–418.
22. Vasilescu DM, Martinez FJ, Marchetti N, Galbán CJ, Hatt C, Meldrum CA, *et al*. Noninvasive imaging biomarker identifies small airway damage in severe chronic obstructive pulmonary disease. *Am J Respir Crit Care Med* 2019;200:575–581.
23. Hume PS, Gibbings SL, McCubbrey AL, Redente EF, Jakubzick C V., Henson PM, *et al*. Stereologic localization of interstitial macrophage subpopulations in human lung [abstract]. *Am J Respir Crit Care Med* 2018;197:A7424.
24. Hume PS, Gibbings SL, Jakubzick C V., Henson PM, Janssen WJ. Localization of interstitial macrophages in human lungs from cigarette smokers and nonsmokers [abstract]. *Am J Respir Crit Care Med* 2019;199:A3766.
25. Mayhew TM, Mühlfeld C, Vanhecke D, Ochs M. A review of recent methods for efficiently quantifying immunogold and other nanoparticles using TEM sections through cells, tissues and organs. *Ann Anat* 2009;191:153–170.
26. Mühlfeld C, Knudsen L, Ochs M. Stereology and morphometry of lung tissue. *Methods Mol Biol* 2013;931:367–390.
27. Melvin NR, Sutherland RJ. Quantitative caveats of standard immunohistochemical procedures: implications for optical disector-based designs. *J Histochem Cytochem* 2010;58:577–584.
28. Mühlfeld C, Hegermann J, Wrede C, Ochs M. A review of recent developments and applications of morphometry/stereology in lung research. *Am J Physiol Lung Cell Mol Physiol* 2015;309:L526–L536.
29. Desch AN, Gibbings SL, Goyal R, Kolde R, Bednarek J, Bruno T, *et al*. Flow cytometric analysis of mononuclear phagocytes in nondiseased human lung and lung-draining lymph nodes. *Am J Respir Crit Care Med* 2016;193:614–626.
30. Tighe RM, Redente EF, Yu Y-R, Herold S, Sperling AI, Curtis JL, *et al*. Improving the quality and reproducibility of flow cytometry in the lung: an Official American Thoracic Society Workshop Report. *Am J Respir Cell Mol Biol* 2019;61:150–161.
31. Gibbings SL, Jakubzick CV. A consistent method to identify and isolate mononuclear phagocytes from human lung and lymph nodes. *Methods Mol Biol* 2018;1799:381–395.
32. Gardella D, Hatton WJ, Rind HB, Rosen GD, von Bartheld CS. Differential tissue shrinkage and compression in the z-axis: implications for optical disector counting in vibratome-, plastic- and cryosections. *J Neurosci Methods* 2003;124:45–59.
33. Dorph-Petersen KA, Nyengaard JR, Gundersen HJGG. Tissue shrinkage and unbiased stereological estimation of particle number and size. *J Microsc* 2001;204:232–246.
34. Weibel ER, Gomez DM. Architecture of the human lung: use of quantitative methods establishes fundamental relations between size and number of lung structures. *Science* 1962;137:577–585.
35. Klein SL, Flanagan KL. Sex differences in immune responses. *Nat Rev Immunol* 2016;16:626–638.
36. Crapo JD, Barry BE, Gehr P, Bachofen M, Weibel ER. Cell number and cell characteristics of the normal human lung. *Am Rev Respir Dis* 1982;126:332–337.
37. Wallace WAH, Gillooly M, Lamb D. Age related increase in the intra-alveolar macrophage population of non-smokers. *Thorax* 1993;48: 668–669.
38. Hoidal JR, Niewoehner DE. Lung phagocyte recruitment and metabolic alterations induced by cigarette smoke in humans and in hamsters. *Am Rev Respir Dis* 1982;126:548–552.
39. Rasp FL, Clawson CC, Hoidal JR, Repine JE. Reversible impairment of the adherence of alveolar macrophages from cigarette smokers. *Am Rev Respir Dis* 1978;118:979–986.
40. Di Stefano A, Capelli A, Lusuardi M, Balbo P, Vecchio C, Maestrelli P, *et al*. Severity of airflow limitation is associated with severity of airway inflammation in smokers. *Am J Respir Crit Care Med* 1998; 158:1277–1285.
41. Wallace WAH, Gillooly M, Lamb D. Intra-alveolar macrophage numbers in current smokers and non-smokers: a morphometric study of tissue sections. *Thorax* 1992;47:437–440.
42. O'Beirne SL, Kikkers SA, Oromendia C, Salit J, Rostmai MR, Ballman KV, *et al*. Alveolar macrophage immunometabolism and lung function impairment in smoking and chronic obstructive pulmonary disease. *Am J Respir Crit Care Med* [online ahead of print] 21 Nov 2019; DOI: 10.1164/rccm.201908-1683LE.
43. Hogg JC, Chu F, Utokaparch S, Woods R, Elliott WM, Buzatu L, *et al*. The nature of small-airway obstruction in chronic obstructive pulmonary disease. *N Engl J Med* 2004;350: 2645–2653.
44. Bharat A, Bhorade SM, Morales-Nebreda L, McQuattie-Pimentel AC, Soberanes S, Ridge K, *et al*. Flow cytometry reveals similarities between lung macrophages in humans and mice. *Am J Respir Cell Mol Biol* 2016;54:147–149.
45. Batdorf BH, Kroft SH, Hosking PR, Harrington AM, Mackinnon AC, Olteanu H. Evaluation of CD43 expression in non-hematopoietic malignancies. *Ann Diagn Pathol* 2017;29:23–27.
46. Westphalen K, Gusarova GA, Islam MN, Subramanian M, Cohen TS, Prince AS, *et al*. Sessile alveolar macrophages communicate with alveolar epithelium to modulate immunity. *Nature* 2014;506: 503–506.
47. Jansing NL, Patel N, McClendon J, Redente EF, Henson PM, Tuder RM, *et al*. Flow cytometry underestimates and planimetry overestimates alveolar epithelial type 2 cell expansion after lung injury. *Am J Respir Crit Care Med* 2018;198:390–392.
48. Ochs M, Nyengaard JR, Jung A, Knudsen L, Voigt M, Wahlers T, *et al*. The number of alveoli in the human lung. *Am J Respir Crit Care Med* 2004;169:120–124.
49. Herring MJ, Putney LF, Wyatt G, Finkbeiner WE, Hyde DM. Growth of alveoli during postnatal development in humans based on stereological estimation. *Am J Physiol Lung Cell Mol Physiol* 2014; 307:L338–L344.